Chemical abundances of planetary nebulae from optical recombination lines – II. The neon abundance of NGC 7009

S.-G. Luo,[1] X.-W. Liu[1,2]* and M. J. Barlow[2]

[1]*Department of Astronomy, Peking University, Beijing 100871, China*
[2]*Department of Physics and Astronomy, University College London, Gower Street, London WC1E 6BT*

ABSTRACT

We present high-quality observations of Ne II optical recombination lines (ORLs) for the bright Saturn Nebula NGC 7009. The measured line fluxes are used to determine Ne^{2+}/H^+ abundance ratios. The results derived from individual multiplets of the 3s–3p and 3p–3d configurations agree reasonably well, although values derived from the 3d–4f transitions, for which only preliminary effective recombination coefficients are available, tend to be higher by a factor of 2 than those derived from the 3–3 transitions – a pattern also seen in other nebulae analysed by us previously. The ORL Ne^{2+}/H^+ abundance ratios of NGC 7009 are found to be higher by a factor of 4 than those derived from the optical collisionally excited lines [Ne III] $\lambda\lambda3868$, 3967 and from the infrared fine-structure lines [Ne III] 15.5 and 36 μm, similar to the patterns found for C, N and O, analysed previously by Liu et al. The result is in line with the general conclusion that while the ratios of heavy-element abundances, derived from ORLs on the one hand and from CELs on the other hand, vary from target to target and cover a wide range from unity to more than an order of magnitude, the discrepancy factor for the individual elements, C, N, O and Ne, is found to be approximately the same magnitude *for a given nebula*, a result which may have a fundamental implication for understanding the underlying physical cause(s) of the large discrepancies between heavy-element abundances derived from these two types of emission line. The result also indicates that while the absolute abundances of heavy elements relative to hydrogen remain uncertain, the abundance ratios of heavy elements, such as C/O, N/O and Ne/O, are probably secure, provided that the same type of emission line, i.e. ORLs or CELs, is used to determine the abundances of both heavy elements involved in the ratio.

For NGC 7009, the total neon abundances derived from the CELs and ORLs, on a logarithmic scale where H = 12.0, are 8.24 ± 0.08 and 8.84 ± 0.25, respectively. The latter is about a factor of 5.5 higher than the solar neon abundance.

Key words: ISM: abundances – planetary nebulae: individual: NGC 7009.

1 INTRODUCTION

Recent determinations of heavy-element abundances relative to hydrogen for planetary nebulae (PN) that have used optical recombination lines (ORLs) have yielded values that are systematically higher than those derived using the traditional method based on the collisionally excited lines (CELs) which dominate nebular spectra. The ratios of heavy-element abundances derived from ORLs on the one hand to those from CELs on the other hand, cover a wide range, from unity (i.e. near agreement) to more than a factor of 20 (Liu et al. 1995, 1999, 2000, 2001b). Comparison of heavy-element abundances derived from these two types of emission line for the limited sample of nebulae studied so far reveals that while the amount of the discrepancy varies from target to target, for a given nebula the magnitude of the discrepancy for individual heavy elements is found to be roughly constant. For example, Liu et al. (1995) determined C, N and O abundances using ORLs for the bright Saturn Nebula NGC 7009 and found that they were all higher than the corresponding CEL values by approximately a factor of 5. Similarly, in NGC 6153 the ORL abundances for C, N, O and Ne are all higher than the corresponding CEL values by a factor of 10 (Liu et al. 2000). Liu et al. (1999) compared C/O abundance ratios derived from the two types of emission line for ten PN and the H II region M 42

*E-mail: xwl@star.ucl.ac.uk

(the Orion Nebula) and found that the C/O abundance ratios derived from ORLs agreed within a factor of 2 with those derived from CELs for the same nebula, even though the O/H abundance ratios derived from these two types of emission line could differ by more than a factor of 20 in the extreme case. This result may have a fundamental implication for understanding the underlying physical cause of the large discrepancies between heavy element abundances derived from ORLs and from CELs, which is currently not well understood, and bears on the interpretation of nebular heavy element abundances in the context of stellar nucleosynthesis and the chemical evolution of galaxies. In other words, while the absolute abundances of heavy elements relative to H may remain uncertain, nebular abundance ratios, such as the C/O, N/O and Ne/O, are probably secure, provided that the abundances of the heavy elements involved in the ratios are derived using the same type of emission line – ORLs or CELs.

In our previous study of NGC 7009, neon was not included in the analysis, partly because of the lack of the necessary atomic data, i.e. effective recombination coefficients for Ne II ORLs, and partly because of the lack of suitable observational data – many of the strongest Ne II ORLs fall in the far-blue wavelength region. Recently, Kisielius et al. (1998) published the effective recombination coefficients of Ne II ORLs, calculated in the *LS*-coupling scheme, for transitions with angular momentum quantum number $l \le 2$. For transitions with $l > 2$, *LS* coupling is no longer a good approximation and additional calculations in an alternative coupling scheme are needed to address these lines, some of which are reasonably strong. However, preliminary effective recombination coefficients for some of the strongest lines from the 3d–4f configuration are available (P. S. Storey, private communication), which are probably accurate to within a factor of 2. These atomic data have been used to determine the ORL Ne/H abundance ratios for NGC 6153 (Liu et al. 2000) and for two bulge PN, M 2-36 and M 1-42 (Liu et al. 2001b).

In this paper, we present observations of Ne II ORLs in NGC 7009 and derive Ne^{2+}/H^+ abundances from them. These are compared with those derived from the optical [Ne III] $\lambda\lambda3868$, 3967 CELs, and from the infrared (IR) [Ne III] 15.5- and 36-μm fine-structure lines.

2   OBSERVATIONS AND DATA REDUCTION

New deep optical spectra of NGC 7009 were obtained during two observing runs at the ESO 1.52-m telescope, in 1995 and 1996 using the long-slit Boller & Chivens spectrograph, and during another two observing runs in 1996 and 1997 at the 4.2-m William Herschel Telescope (WHT), using the ISIS long-slit double spectrograph. An observational journal is given in Table 1. During the 1995 ESO 1.52-m run, the B&C spectrograph was used with a Ford 2048×2048 15 μm $\times$ 15 μm charge-coupled device (CCD). The slit was positioned at PA $= 79°$, i.e. along the nebular major-axis and passing through the two outlying ansae (cf. the WFPC2 image of NGC 7009 published by Balick et al. 1998), and was offset 2–3-arcsec south of the central star (CS) in order to avoid the strong continuum emission from the CS, which reduces the signal-to-noise ratio (S/N) and the detectability of weak emission lines. The slit was about 3.5-arcmin long. A 2-arcsec slit width was used for all nebular observations except for one short exposure aimed at measuring the CS continuum flux distribution, for which an 8-arcsec wide slit was used, with the slit centred on the CS. In 1996 the CCD on the B&C spectrograph was replaced by a thinned ultraviolet-(UV-) enhanced Loral 2048×2048 15 μm $\times$ 15 μm chip of much improved quantum efficiency. For both observing runs at the ESO 1.52-m telescope, in order to reduce the read-out noise, the CCD was binned by a factor of 2 along the slit direction, yielding a spatial sampling of 1.63 arcsec pixel^{-1} projected on the sky. Several wavelength regions between the near-UV atmospheric cut-off to approximately 5000 Å were observed using a 2400 line mm^{-1} holographic grating, which yields a spectral resolution of approximately 1.5 Å FWHM. Lower resolution spectra from 3520 to 7420 Å were also obtained using a 600 groove mm^{-1} grating. The *Hubble Space Telescope* (*HST*) standard stars, Feige 110 and (the nucleus of the PN) NGC 7293, were observed with an 8-arcsec wide slit for the purpose of flux calibration.

Observations at the WHT 4.2-m telescope were obtained using the ISIS double spectrograph. For both the Blue and Red Arms, a Tek 1024×1024–24 μm $\times$ 24 μm chip was used, which yielded a spatial sampling of 0.3576 arcsec pixel^{-1} projected on the sky. In 1996, 600 and 316 groove mm^{-1} gratings were used in the Blue and Red Arms, respectively. In 1997, they were replaced by 1200 and 600 groove mm^{-1} gratings, respectively. During the 1996 WHT run, the slit was scanned across the whole nebula by uniformly driving the telescope differentially in right ascension. The observations thus yield average spectra for the whole nebula, which, when combined with the total Hβ flux published in the literature, measured with a large entrance aperture, then yield

Table 1. Journal of observations. All observations were taken with a 2-arcsec wide slit unless otherwise specified.

Date (UT)	Telescope	λ range (Å)	FWHM (Å)	PA (deg)	Exp. time (s)
30/07/95	ESO1.5 m	3520–7420	4.5	79	2×30, 60, 60[a], 1200
30/07/95	ESO1.5 m	4000–4980	1.5	79	2×300, 900, 1418, 5×1800
12/07/96	ESO1.5 m	3040–4048	1.5	79	5×1800
08/07/96	ESO1.5 m	3994–4983	1.5	79	5, 60, 100, 400, 900, 2×1800
10/07/96	WHT4.2 m	3617–4434	2.4	Scanned	2×20, 2×600
10/07/96	WHT4.2 m	4190–4990	2.4	Scanned	3×10, 2×20, 300, 2×600
10/07/96	WHT4.2 m	5176–6709	4.5	Scanned	3×10, 2×20, 300, 2×600
11/08/96	WHT4.2 m	6484–8007	4.5	Scanned	2×20, 2×600
11/08/97	WHT4.2 m	4104–4512	1.2	79	30, 120, 1200, 432
11/08/97	WHT4.2 m	4507–4918	1.2	79	30, 1200
11/08/97	WHT4.2 m	5165–5967	2.4	79	30, 120, 1200, 428
11/08/97	WHT4.2 m	6002–6810	2.4	79	30, 1200

[a] Observed with an 8-arcsec wide slit.

absolute fluxes of the whole nebula for all the emission lines detected in the spectra. The spectra obtained in the 1997 run were obtained with a fixed slit oriented at PA $= 79°$ and passing through the CS. For both WHT runs, a 1-arcsec wide slit was used for nebular observations. Two *HST* spectrophotometric standard stars, BD $+28° 4211$ and HZ 44, were observed using a 6-arcsec wide slit for the purpose of flux calibration.

All the spectra were reduced with standard procedures using the LONG92 package in MIDAS[1]. The spectra were bias-subtracted, flat-fielded, cosmic rays removed and wavelength-calibrated using exposures of comparison lamps, and then flux-calibrated using wide slit observations of spectrophotometric standard stars. Ozone absorption bands that affect the ESO 1.52-m data shortwards of 3400 Å were corrected for using observations of the standard stars Feige 110 and the CS of NGC 7293 taken with a 2-arcsec wide slit.

Infrared spectra from 2.4 to 45 μm have been obtained for NGC 7009 with the Short Wavelength Spectrometer (SWS) on-board the *Infrared Space Observatory* (*ISO*) during *ISO* Orbit #344 on 1996 October 25 (product ID 34 400 518) and #738 on 1997 November 23 (product ID 73 801 242), as part of an *ISO* LWS Guaranteed Time programme. The spectra were taken with the Astronomical Observing Template (AOT) SWS01 in full grating scan mode with a spectral resolution of approximately 500. The total on-target observing times were, respectively, 1192 and 2124 s for the two observations. A full list of fluxes of lines detected in these spectra will be published elsewhere together with other PN observed in this programme (Barlow et al., in preparation). For completeness, we include the fluxes of the [Ne II] 12.8-μm and the [Ne III] 15.5- and 36-μm fine-structure lines obtained from these observations in our current analysis of the neon abundance in NGC 7009.

The SWS observation 73 801 242 yields a flux of 3.90×10^{-10} and 3.49×10^{-11} erg cm^{-2} s^{-1} for the 15.5- and 36-μm lines, respectively. The corresponding values derived from observation 34 400 518 are 3.76×10^{-10} and 4.09×10^{-11} erg cm^{-2} s^{-1}. The SWS has rectangular entrance aperture the size of which varies depending on the wavelength band and was 14×27 arcsec^2 (band 3A) and 20×33 arcsec^2 (band 4) for the [Ne III] 15.5- and 36-μm lines, respectively. The observations were unfortunately carried out with the major axis of the aperture oriented at PA $= 162$ and $164°$ for observations 73 801 242 and 34 400 518, respectively, i.e. approximately parallel to nebular minor axis (in PA $= 169°$). This leads to a significant loss of light, in particular for the 15.5-μm line. A further complication arose from the fact that the pointing of the telescope during observation 34 400 518 was displaced from the centre of NGC 7009 by 8.7-arcsec south. However, given the geometry of the entrance aperture and their particular orientation during the observations, observation 34 400 518 caught a similar area of the bright inner nebulosity as observation 73 801 242, where the latter was correctly positioned. Here we will adopt the fluxes measured from observation 73 801 242.

The fraction of the [Ne III] emission captured by the SWS observations can be estimated using the [O III] $\lambda5007$ image of NGC 7009 obtained recently with WFPC2 on the *HST* (Rubin et al., private communication). Assuming that the [Ne III] emitting zone has a similar spatial extension as that of [O III], we find that for the SWS observation 73 801 242, the SWS entrance aperture should have received, respectively, 69 and 86 per cent of the total fluxes in the [Ne III] 15.5- and 36-μm lines emitted by NGC 7009. These two values are probably slightly underestimated, given that Ne$^+$

has an ionization potential of 41.0 eV, slightly higher than the corresponding value of 35.1 eV for O$^+$. However, the uncertainties thus introduced are likely to be small. After correcting for the effects of finite aperture, we estimate that NGC 7009 should have fluxes of 5.65×10^{-10} and 4.06×10^{-11} erg cm^{-2} s^{-1} for the [Ne III] 15.5- and 36-μm lines, respectively. These fluxes will be adopted for our abundance analysis.

Rubin et al. (1997) measured the fluxes of several infrared fine-structure lines from NGC 7009 with the *Kuiper Airborne Observatory* (*KAO*). The entrance aperture of the *KAO* spectrometer had a FWHM beam size of approximately 40 arcsec, big enough to encompass the entire emitting region of NGC 7009. Unfortunately, the [Ne III] 15.5-μm line cannot be measured at *KAO* altitude, while for the 36-μm line, only a flux upper limit of 1.2×10^{-10} erg cm^{-2} s^{-1} was obtained. The [S III] 18.7-μm line was well detected by them with a measured flux of $(8.80 \pm 1.00) \times 10^{-11}$ erg cm^{-2} s^{-1} for the whole nebula. The SWS has the same aperture size of 14×27 arcsec^2 at 15.5 and 18.7 μm and observation 73 801 242 yields a [Ne III] 15.5- to [S III] 18.7-μm line flux ratio of 6.7 ± 0.2. Thus if we assume that the [Ne III] and [S III] emitting regions are co-spatial, then this ratio together with the total [S III] 18.7-μm line flux measured by the *KAO* yield a [Ne III] 15.5-μm flux of $(5.9 \pm 0.7) \times 10^{-10}$ erg cm^{-2} s^{-1} for the entire nebula of NGC 7009, in good agreement with the estimate obtained above.

The [Ne II] 12.8-μm fine-structure line has been well detected by the *ISO* SWS and its flux from observation 73 801 242 is 7.90×10^{-12} erg cm^{-2} s^{-1}. The line was observed in the same band (3A) as the [Ne III] 15.5-μm line, i.e. both were measured with an entrance aperture of 14×27 arcsec^2. In order to obtain the 12.8-μm line flux for the whole nebula, we make use of Brα 4.05 μm, also detected by the SWS with a flux of 7.05×10^{-12} erg cm^{-2} s^{-1}. The Brα line was observed in band 1E with an entrance aperture of 14×20 arcsec^2. Because of the specific orientation of the SWS aperture, PA $= 162°$, roughly parallel to the nebular minor-axis and given the fact that NGC 7009 has an angular diameter of only ~23 arcsec in this direction, the SWS apertures for band 3A and 1E covered essentially the same area of the nebular surface and thus no correction is needed to account for the different aperture sizes of band 3A and 1E for this particular observation. For an electron temperature of 7100 K and a density of 3930 cm^{-3}, $I(\text{Br}\alpha)/I(\text{H}\beta) = 0.0886$ (Storey & Hummer 1995). Thus for a total intrinsic Hβ flux of $\log I(\text{H}\beta) = -9.65$ (erg cm^{-2} s^{-1}; cf. Section 3.1), we have $I(\text{Br}\alpha) = 1.98 \times 10^{-11}$ erg cm^{-2} s^{-1} for the entire nebula. This together with the [Ne II] 12.8-μm to Brα flux ratio measured with the SWS yields a total [Ne II] 12.8-μm line flux of 2.22×10^{-11} erg cm^{-2} s^{-1} for NGC 7009, which will be adopted in the following analysis[2].

Table 2 summarizes the intensities of all the optical and IR CELs

---

[1] MIDAS is developed and distributed by the European Southern Observatory.

[2] From the observed [Ne III] 15.5-μm to Brα intensity ratio of 55.3 measured by the SWS without correcting for the aperture effects, and the total Brα flux of 1.98×10^{-11} erg cm^{-2} s^{-1}, we obtain a total [Ne III] 15.5-μm line flux of 1.10×10^{-9} erg cm^{-2} s^{-1}, about a factor of 2 higher than the two estimates given above. Such a high flux would imply that the SWS had captured only 35 per cent of the total [Ne III] 15.5-μm line flux emitted by NGC 7009, a value that seems unrealistically small. The cause of the discrepancy is unclear. One possibility is that it is related to the uncertainties in the beam profiles of the SWS for different bands – the beam profiles deduced from observations of bright stars may not be applicable to extended sources with a complex spatial structure such as NGC 7009 (Leech 2000).

of neon that will be used to derive the ionic abundances presented in the next section.

3 RESULTS AND DISCUSSION

3.1 Plasma diagnostics

The observed Balmer line ratios, Hα/Hβ, Hγ/Hβ and Hδ/Hβ, from the ESO 1.52-m observations yield an average logarithmic extinction at Hβ of $c = 0.07$, which will be used to correct all the optical line fluxes. This value is smaller than the value of 0.2 deduced by Liu et al. (1995). This may partly be caused by the different regions of the nebula being sampled – the data analysed by Liu et al. (1995) were dominated by light from the nebular minor-axis. However, the possibility that the discrepancy is caused by calibration uncertainties cannot be ruled out. The results presented here are, however, hardly affected by the small uncertainties in the adopted reddening correction.

Condon & Kaplan (1998) give a radio 1.4-GHz flux density of 0.683 Jy for NGC 7009. This together with its absolute Hβ flux (Cahn, Kaler & Stanghellini 1992), $\log F(H\beta) = -9.80$ (erg cm^{-2} s^{-1}), the electron temperature of 7100 K derived from the nebular continuum Balmer discontinuity, and the He$^+$/H$^+$ and He^{2+}/H$^+$ abundance ratios (see below), yield an extinction constant $c = 0.15$, leading to a reddening-corrected Hβ flux of $\log I(H\beta) = -9.65$ (erg cm^{-2} s^{-1}). The latter value will be used to normalize the infrared [Ne III] 15.5- and 36-μm line fluxes to Hβ. The normalization procedure for the IR lines is equivalent to normalizing the IR line fluxes to the radio continuum flux density, both are unaffected by reddening. After the normalization, the [Ne II] 12.8-μm line and the [Ne III] 15.5- and 36-μm lines have intensities of 9.93, 250 and 18.0, respectively, on a scale where $I(H\beta) = 100$.

The electron temperatures and densities derived from several standard plasma diagnostic line ratios are presented in Table 3. The electron densities derived from optical density diagnostics, such as the [O II] $\lambda 3729/\lambda 3726$, [Ar IV] $\lambda 4740/\lambda 4711$, [Cl III] $\lambda 5537/\lambda 5517$ and [S II] $\lambda 6731/\lambda 6716$ doublet ratios, agree

Table 2. Intensities of neon optical and IR CELs.

Line	Intensity (Hβ = 100)
[Ne II] 12.8 μm	9.9 ± 3.0
[Ne III] $\lambda 3868$	110 ± 6
[Ne III] $\lambda 3967$	32.2 ± 1.6
[Ne III] 15.5 μm	250 ± 12
[Ne III] 36.0 μm	18.0 ± 1.8
[Ne IV] $\lambda\lambda 4724, 4725$	0.030 ± 0.003

remarkable well, with an average value of 3930 cm^{-3}. On the other hand, the [O III] far-IR fine-structure 52-/88-μm line ratio yields a lower density of 1260 cm^{-3}, owing to the fairly low critical densities of the 52- and 88-μm lines (Liu et al. 2001a). The [Ne III] 15.5- and 36-μm fine-structure lines have much higher critical densities (2.9×10^4 and 2.0×10^5 cm^{-3}) than the 52- and 88-μm lines, comparable to those of the [Ar IV] and [Cl III] optical doublets, and are therefore unlikely to be affected by modest density inhomogeneities that may be present in NGC 7009. The 15.5-/36-μm flux ratio measured with the SWS, after correction for the aperture effects (cf. Section 2), yields an electron density of 11 500 cm^{-3}, with a possible range of 2000–23 000 cm^{-3}.

The [O III] nebular to auroral line ratio $\lambda 4959/\lambda 4363$ yields an electron temperature of 9980 K, significantly higher than the values derived from the ratios of the [Ne III] and [O III] infrared fine-structure lines to corresponding optical forbidden lines. The electron temperature derived from the ratio of the nebular continuum Balmer discontinuity to H11 is even lower. The [O III] $\lambda 4959/\lambda 4363$ temperature in Table 3 was calculated for an electron density of 3930 cm^{-3}, i.e. the average density derived from optical density diagnostic ratios. For the [Ne III] and [O III] infrared fine-structure line to optical forbidden line ratios in Table 3, the electron temperatures were deduced assuming an electron density of 1260 cm^{-3}, the value yielded by the [O III] fine-structure 52-/88-μm line ratio (Liu et al. 2001a). Owing to the fairly high critical densities of the lines involved, the electron temperatures deduced from the $\lambda 4959/\lambda 4363$ and (15.5 μm + 36 μm)/($\lambda 3868 + \lambda 3967$) ratios differ little for the two adopted densities. In contrast, the electron temperature derived from the [O III] (52 μm + 88 μm)/$\lambda 4959$ ratio is quite sensitive to the electron density assumed – for $N_e = 3930$ cm^{-3}, the observed ratio yields an electron temperature of 6730 K, versus 8350 K if $N_e = 1260$ cm^{-3}.

The electron temperature derived from the Balmer jump has a weak dependence on the helium ionic abundance. The value presented in Table 3 was derived assuming He^{2+}/H$^+$ = 0.011, deduced from the observed intensity of the He II $\lambda 4686$ line, together with He$^+$/H$^+$ = 0.093, the average value deduced from the He I $\lambda\lambda 4471$, 5876, 6678 lines. The Balmer jump temperature of 7100 K is lower than the average value of 8200 K obtained by Liu et al. (1995) and 8700($-1100, +1500$) K obtained by Liu & Danziger (1993) for this nebula, but is probably consistent with the latter two measurements within the uncertainties. The current determination is probably more accurate given the much higher signal-to-noise ratio and spectral resolution of the current observations and the fact that it was calculated from the ratio of the Balmer jump to H11, rather than from the ratio of the Balmer jump to Hβ used by Liu et al. (1995) and Liu & Danziger (1993). Consequently, the current result is less sensitive to possible uncertainties in the reddening corrections.

Table 3. Plasma diagnostics.

Diagnostic	Ratio	T_e (K)
[O III] $\lambda 4959/\lambda 4363$	53.1 ± 3.0	9980 ± 180
[O III] (88 μm + 52 μm)/$\lambda 4959$	1.33 ± 0.07	8350 ± 150
[Ne III] (15.5 μm + 36 μm)/($\lambda 3868 + \lambda 3967$)	1.89 ± 0.20	9050 ± 250
BJ/H II (Å^{-1})	0.144 ± 0.014	7100 ± 1200
Diagnostic	Ratio	N_e (cm^{-3})
[Ne III] 15.5 μm/36 μm	13.9 ± 2.1	11 500 (2–23) $\times 10^3$
[O II], [S II], [Ar IV], [Cl III] opt. dblt ratios		3930 ± 300

The fact that the [O III] $\lambda 4959/\lambda 4363$ ratio yields an electron temperature that is significantly higher than the values yielded by the other temperature diagnostics listed in Table 3 suggests that NGC 7009 may have significant temperature fluctuations (Peimbert 1967, 1971). In terms of Peimbert's mean temperature T_0 and temperature fluctuation parameter t^2, the observed [O III] $\lambda 4959/\lambda 4363$ temperature of 9980 K and the Balmer jump temperature of 7100 K yield $T_0 = 7900$ K and $t^2 = 0.061$. The latter is equivalent to a fluctuation amplitude of 25 per cent around the mean temperature.

3.2 The Ne^{2+}/H^+ abundance ratio from ORLs

Several dozen Ne II optical recombination lines have been detected. The measured line intensities, after correction for reddening and normalized such that $I(H\beta) = 10^4$, together with the Ne^{2+}/H^+ abundance ratios derived from them, are presented in Tables 4 and 5 for transitions from the 3s–3p and 3p–3d configurations and for transitions from the 3d–4f configuration, respectively. An electron temperature of 7100 K, as derived from the Balmer discontinuity, was assumed. Many of the 3s–3p and 3p–3d transitions fall in the far-blue wavelength region and a spectrum showing this wavelength region is plotted in Fig. 1, with

the detected Ne II lines marked. Transitions from the 3d–4f configuration fall at longer wavelengths. Two segments of spectra showing the wavelength regions from 4210 to 4260 and 4380 to 4465 Å are plotted in Fig. 2. The latter includes the strongest Ne II line from the 3d–4f configuration, 3d $^4F_{9/2}$–4f $2[5]^o_{11/2}$ $\lambda 4391.99$ (multiplet V55e).

Apart from the lines listed in Tables 4 and 5, several additional Ne II lines have been detected. These lines are, however, either very weak or blended with stronger lines of other ionic species. They were therefore excluded from the abundance analysis. They include, for example, $\lambda 3388.42$ (3p $^2D^o_{3/2}$–3d $^2F_{5/2}$, V 20), $\lambda 3416.91$ (3p $^2D^o_{5/2}$–3d $^2D_{5/2}$, V 21), $\lambda 3357.82$ (3p $^4D^o_{5/2}$–3d $^4D_{5/2}$, V 12). The $\lambda 3297.73$ line of multiplet V 1 falls in the wing of the strong O III Bowen fluorescence line $\lambda 3299.36$. Also falling near this wavelength are two C II lines, 4d ^2D–3d' $^2D^o$ $\lambda\lambda 3298.01$, 3298.09, the contribution of which is difficult to estimate. The intensity of the Ne II $\lambda 3297.73$ line is therefore quite uncertain and probably has been overestimated. It was thus excluded when calculating the total intensity of multiplet V 1. Both transitions from multiplet V 9, 3s' ^2D–3p' $^2F^o$ $\lambda\lambda 3568.50$, 3574.18, which have an excited state parentage of $2s^2 2p^4 {}^1D$, have been detected. The ionic abundance derived from this multiplet is, however, much higher than yielded by other multiplets. Similar discrepancies are

Table 4. Ne^{2+}/H^+ abundances from the Ne II 3s–3p and 3p–3d transitions.

λ_0 (Å)	Mult	I_{obs} (H$\beta = 10^4$)	$10^4 \times Ne^{2+}/H^+$	I_{obs} (H$\beta = 10^4$)	$10^4 \times Ne^{2+}/H^+$
		ESO 1.52-m Data PA $= 79°$		WHT 1997 Scanned Data	
3694.21	V 1	29.4	8.97	22.4	6.81
3709.62	V 1	11.0	8.49	9.73	7.49
3766.26	V 1	9.10	6.60	4.87	3.53
3777.14	V 1	4.51	3.54	5.87	4.60
V 1 3s ^{4}P–3p ^{4}P		69.43	7.45	55.1	5.92
3334.84	V 2	34.5	5.14		
3355.02^a	V 2	29.6	5.89		
3297.73^b	V 2	15.0	9.80		
V 2 3s ^{4}P–3p ^{4}D		90.4	5.39		
3481.93	V 6	5.10	5.52		
V 6 3s ^{2}P–3p ^{2}S		7.65	5.52		
3329.16	V 12	4.64	7.67		
V 12 3p ^{4}D–3d ^{4}D		13.5	7.67		
3213.73, 14.33	V 13	8.62	2.81	13.5	4.38
3218.19^c	V 13	22.9	5.45		
3244.09	V 13	5.76	2.02		
V 13 3p ^{4}D–3d ^{4}F		43.3	3.68	52.0	4.38
3367.22	V 20	11.0	3.38		
V 20 3p ^{2}D–3d ^{2}F		19.2	3.38		
3416.91^d	V 21	8.25	13.0	16.4	25.8
3453.07	V 21	1.72	4.25		
V 21 3p ^{2}D–3d ^{2}D		4.76	4.25		
3456.61	V 28	3.34	4.08		
V 28 3p ^{2}S–3d ^{2}P		5.00	4.08		
3542.8	V 34	3.25	2.89		
3564.9	V 34	2.43	3.25		
V 34 3p ^{4}S–3d ^{4}P		6.81	3.05		

^{a} Corrected for the contribution from the He I 2s ^{1}S – 7p ^{1}P $\lambda 3354.54$ line.
^{b} Intensity probably overestimated; not included in calculating the total intensity of the multiplet.
^{c} Neglecting a small contribution from Ne II 3p $^4D^o_{3/2}$–3d $^4P_{1/2}$ $\lambda 3217.30$ (about 3 per cent).
^{d} Blended with the O III Bowen fluorescence line $\lambda 3415.29$ and Ne II $2s^2 2p^4({}^3P)3p$ $^2D^o_{5/2}$–$2s^2 2p^4({}^3P)3d$ $^4F_{7/2}$ $\lambda 3417.69$ and thus excluded in calculating the total intensity of multiplet V 21.

Table 5. Ne^{2+}/H^+ abundances from the 3d–4f transitions.

λ_0 (Å)	Mult.	ESO 1.52-m data PA = 79°		WHT 1996 Scanned data		WHT 1997 data PA = 79°	
		I_{obs} (Hβ = 10^4)	$10^4 \times Ne^{2+}/H^+$	I_{obs} (Hβ = 10^4)	$10^4 \times Ne^{2+}/H^+$	I_{obs} (Hβ = 10^4)	$10^4 \times Ne^{2+}/H^+$
4219.74[a]	V 52a	6.74	12.6	6.99	13.1	6.16	11.5
4233.85	V 52a	1.52	11.4	1.85	13.8	1.52	11.4
4231.64[b]	V 52b	2.44	19.2	3.28	25.9	2.37	18.6
4391.99[c]	V 55e	7.28	7.53	7.79	8.06	7.13	7.38
4409.30	V 55e	6.31	9.80	6.15	9.55	6.24	9.72
4397.99	V 57b	2.19	6.56	1.84	5.51	1.85	5.54
4428.64[d]	V 60c	4.83	11.5	4.51	10.5	4.79	11.4
4430.94[e]	V 61a	3.31	12.1	3.40	12.5	3.17	11.6
4457.05[bf]	V 61a	2.50	26.3	2.47	25.9	2.11	22.2
4413.22[g]	V 65	2.96	12.9	2.43	10.6	2.71	11.8
4250.64[b]	V 52b	1.69	19.9	1.54	18.1	1.21	14.2
Sum		35.1	9.93	35.0	9.88	33.6	9.49

[a] Neglecting Ne II 3d $^4D_{7/2}$–4f 2[4]$_{7/2}$ λ4219.37 (V 52a), which may contribute a few per cent of the observed intensity.
[b] Not included in calculating the total intensity and the average abundance given in the last row.
[c] Neglecting Ne II 3d $^4F_{9/2}$–4f 2[5]$_{9/2}$ λ4392.00 (V 55e).
[d] Including the contributions from Ne II 3d $^2D_{5/2}$–4f 2[3]$_{7/2}$ λ4428.52 (V 61b); but neglecting Ne II 3d $^2F_{5/2}$–4f 1[3]$_{5/2}$ λ4428.52 (V 60c).
[e] Including Ne II 3d $^4F_{3/2}$–4f 1[2]$_{5/2}$ λ4430.90 (V 57a).
[f] Neglecting Ne II 3d $^2D_{3/2}$–4f 2[2]$_{3/2}$ λ4457.24 (V 61d).
[g] Neglecting Ne II 3d $^4P_{5/2}$–4f 0[3]$_{5/2}$ λ4413.11 (V 65) and 3d $^4F_{3/2}$–4f 1[3]$_{5/2}$ λ4413.11 (V 57c).

observed in another two PN, M 1-42 and M 2-36 (Liu et al. 2001b). Given that the transitions of this multiplet involve two excited electrons, it is possible that their excitation is dominated by dielectronic recombination and that the effective recombination coefficients adopted in the current analysis have been underestimated. We have therefore excluded this multiplet from our analysis.

The 3s $^4P_{3/2}$–3p $^4D^o_{5/2}$ λ3355.02 line of multiplet V 2 is blended with He I 2s ^{1}S–7p ^{1}P^o λ3354.55 and the contribution from the latter line was corrected for using the observed intensity of the He I 2s ^{1}S–5p^{1}P^o λ3613.64 line, assuming $I(\lambda3355)/I(\lambda3614) = 0.35$ (Brocklehurst 1972). The correction amounts to 30 per cent. The Ne II λ3218.19 line of multiplet V 13 blends with several other weak Ne II and O II recombination lines. However, the total contribution from these weak lines is estimated to be only a few per cent and has therefore been neglected.

The ionic abundances presented in Table 4 were derived using the effective recombination coefficients of Kisielius et al. (1998), calculated in *LS* coupling. We have assumed case A recombination for the quartets and case B for the doublets. The ionic abundances derived from the quartets are insensitive to optical depth effects. In contrast, except for multiplet V 20, the case A effective recombination coefficients of the doublets V 6, V 21 and V 28 are lower than their corresponding case B values by factors of 7.6, 16.4 and 9.2, respectively. The average ionic abundance derived from the quartets and the case-insensitive V 20 doublet is 5.10×10^{-4}, comparable to the mean of 4.62×10^{-4} derived from V 6, V 21 and V 28, suggesting that case B is a good approximation for the doublet transitions.

For the 3d–4f transitions, only preliminary effective recombination coefficients, calculated in intermediate coupling for a single electron temperature of 10 000 K, are available (P. J. Storey, private communication). The ionic abundances presented in Table 5 were calculating assuming an electron temperature of 10 000 K for Ne II lines *and* Hβ. Given the fact that the effective recombination coefficients for all radiative recombination lines have only a weak, similar power-law dependence on electron temperature,

$\alpha_{eff} \propto T_e^{-\beta}$, where $|\beta| \sim 1$, the errors introduced by adopting a nominal electron temperature of 10 000 K, rather than the actual value of 7100 K derived from the nebular continuum Balmer discontinuity, are likely to be small compared with other possible uncertainties, including the observational errors. For example, for the 3s–3p and 3p–3d multiplets listed in Table 4, for which detailed calculations of their effective recombination coefficients are available for a wide range of electron temperature from 1000 to 20 000 K, the ionic abundances derived from them for an electron temperature of 10 000 K differ by less than 2 per cent from those presented in Table 4, deduced for an electron temperature of 7100 K.

The total intensities of the 3d–4f transitions listed in Table 5 are given in the last row of Table 5. Three transitions, $\lambda\lambda$4231.64, 4457.05 and 4250.64, were excluded, because they yield abnormally high abundances. In the case of NGC 6153 analysed previously by Liu et al. (2000), the latter two lines also yield much higher abundances than other 3d–4f transitions and were rejected by Liu et al. (2000). It is possible that some unknown lines are contaminating their observed intensities, although no convincing candidates for the blended lines can be identified. For the three data sets, 'ESO 1.52-m Data PA = 79°', 'WHT 1996 Scanned Data' and 'WHT 1997 Data PA = 79°', the ionic abundances yielded by the co-added total intensities of the 3d–4f transitions are, 9.93, 9.88 and 9.49×10^{-4}, respectively, which will be adopted as the average abundances from the 3d–4f transitions. For comparison, the corresponding average ionic abundances derived from the individual 3d–4f transitions, equally weighted, are 10.6, 10.5 and 10.0×10^{-4} from the three data sets, respectively.

Comparison of Tables 4 and 5 shows that the ionic abundances derived from the 3d–4f transitions are systematically higher than those derived from the 3s–3p and 3p–3d multiplets, by approximately a factor of 2. Similar discrepancies are observed for the other three nebulae analysed by us, NGC 6153 (Liu et al. 2000), and M 1-42 and M 2-36 (Liu et al. 2001b). The ratios of the average abundance derived from the 3d–4f lines to the average values yielded by the 3s–3p and 3p–3d multiplets are 2.0, 2.0,
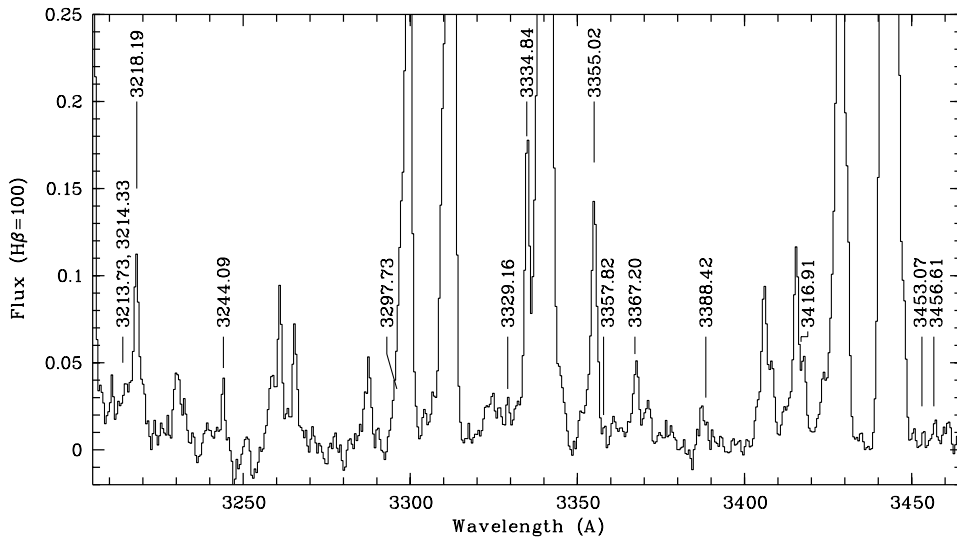
Figure 1. Spectrum of NGC 7009 from 3200 to 3460 Å obtained at the ESO 1.52-m telescope. The spectrum was corrected to a laboratory wavelength rest-frame and normalized such that $F(H\beta) = 100$. The flux has not been corrected for interstellar extinction.
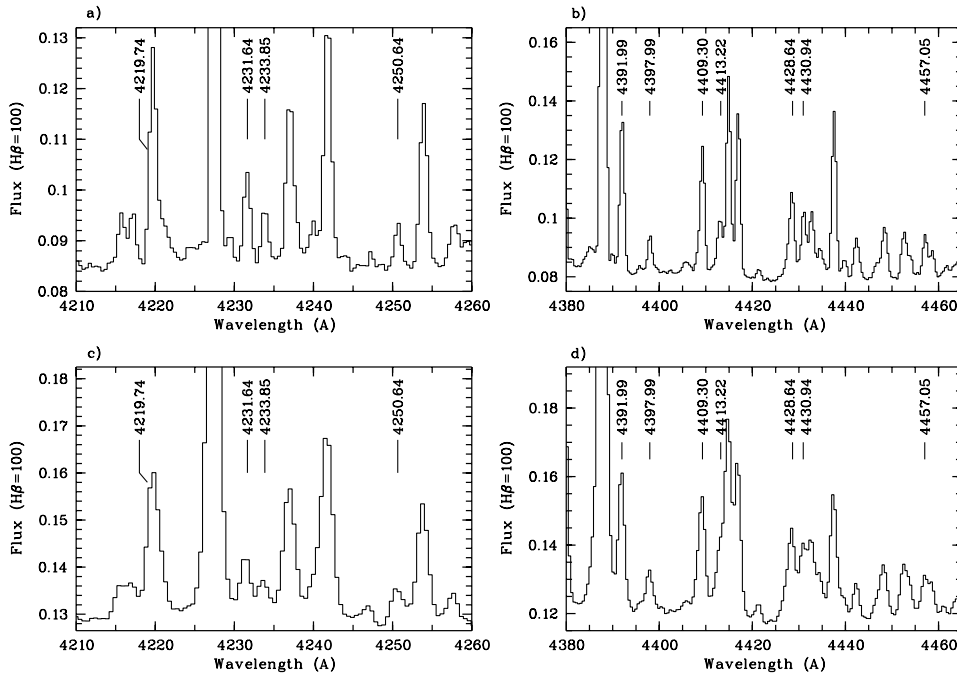

Figure 2. Same as Fig. 1 but for the wavelength regions from 4210 to 4260 and 4380–4460 Å. Panels (a) and (b) are from the 1997 WHT 4.2-m data, while panels (c) and (d) are from the ESO 1.52-m data.

1.7 and 1.4 for NGC 7009, M 2-36, NGC 6153 and M 1-42, respectively. The near constancy of this disparity between average ionic abundances derived from the 3–3 transitions and from the 3d–4f transitions among the four nebulae is in sharp contrast with the large variations in the magnitude of the discrepancies between the ionic abundances derived from ORLs on the one hand and from CELs on the other, which span a wide range, from a factor of 4 to a factor 20 for these nebulae. A nearly identical disparity is found between the O II 3–3 and 3d–4f ORLs. The cause of the disparity is unknown, although it is clear that it cannot be caused by effects such as observational uncertainties, line blending or fluorescence (line or continuum).

The average Ne^{2+}/H^+ abundance derived from the 3d–4f transitions for the three data sets presented in Table 5 is

9.77×10^{-4}. We will adopt this value as the mean Ne^{2+}/H^+ abundance ratio from 3d–4f transitions.

3.3 Comparison with abundances derived from CELs

For an electron temperature of 9980 K, as derived from the [O III] nebular to auroral forbidden line ratio (Table 3), the [Ne III] optical forbidden lines, $\lambda\lambda 3868, 3967$, and the infrared fine-structure lines, 15.5 and 36 μm (Table 2), yield Ne^{2+}/H^+ abundance ratios of 1.10 and 1.63×10^{-4}, respectively. Here an electron density of $3930 \, cm^{-3}$ has been assumed. The results are essentially identical for $N_e = 1260 \, cm^{-3}$, given the high critical densities of the [Ne III] lines. The slightly lower abundance derived from the optical $\lambda\lambda 3868, 3967$ lines is consistent with the fact that the electron

temperature derived from the ratio of the [Ne III] fine-structure lines to the optical nebular lines, $T_e = 9050$ K, is lower than the value of 9980 K deduced from the [O III] $\lambda 4959/\lambda 4363$ ratio. Together with the even lower Balmer jump temperature, this points to the possibility that NGC 7009 may have significant temperature fluctuations.

If we average the Ne^{2+}/H^+ ionic abundance ratios derived from the individual 3s–3p and 3p–3d *multiplets* and from the *total* intensity of the 3d–4f transitions, as done by Liu et al. (1995) in their analysis of the O II ORLs from NGC 7009, we obtain a mean ORL Ne^{2+}/H^+ abundance of 5.44×10^{-4}, which is a factor of 4.0 higher than the average Ne^{2+}/H^+ abundance ratio of 1.37×10^{-4} derived from the [Ne III] optical forbidden lines and infrared fine-structure lines. Considering the factor-of-two disparity between the ORL Ne^{2+}/H^+ abundances yielded by the 3–3 transitions and by the 3d–4f lines, and the modest difference between the CEL values deduced from the [Ne III] optical forbidden lines and infrared fine-structure lines, the ratio of ORL to CEL Ne^{2+}/H^+ abundances may span a range from 3 to 9.

Liu et al. (1995) compared the ionic abundances of C, N and O derived from ORLs and CELs in NGC 7009 and found that the ORL abundances were systematically higher than the corresponding CEL values by factors of 6.1, 4.1 and 4.7, respectively, or roughly a factor of 5 for all the three elements. The current study shows that this large disparity between the ORL and CEL abundances recurs in the case of neon to a remarkable degree of similarity. This recurring disparity between the ionic abundances derived from these two types of emission line, by approximately the same factor for all of the elements studied in NGC 7009, is even more severe in the case of NGC 6153 where, the ORL C, N, O and Ne abundances are all higher than the corresponding CEL values by a factor of 10. In fact, Liu et al. (1999) compared the C and O abundances derived from ORLs and CELs for a sample of 11 nebulae, including ten PN and the H II region M 42, and found that while the ratios of O^{2+}/H^+ abundances derived from ORLs to those from CELs span a wide range, from near unity to over a factor of 20, the C^{2+}/O^{2+} abundance ratios yielded by these two types of emission line are nearly identical within a factor of about 2.

Liu et al. (2000) considered a variety of hypotheses that might account for the factor-of-10 disparity between the heavy-element abundances derived from ORLs and CELs in the case of NGC 6153 and showed that a two-component nebular model, with H-deficient condensations or filaments embedded in diffuse material of more or less 'normal' metallicity, can account for many of the observed properties of NGC 6153. Whether this interpretation can account for similar disparities that have been observed in many other planetary nebulae remains to be seen. Unless the underlying physical cause of such large disparities is understood, the abundances of heavy elements, *relative to hydrogen*, derived from nebular analyses remain uncertain. However, our analyses seem to indicate that the relative abundances of heavy elements, such as C/O, N/O and Ne/O ratios, are probably secure, provided the same type of emission line, either CELs or ORLs, is used to derive the abundances of both heavy elements involved in the ratio.

3.4 Total elemental Ne/H abundance ratios from ORLs and CELs

In order to obtain the total elemental Ne/H abundance ratio, we need to know the concentrations in the Ne^+ and Ne^{3+} ionization stages. From the flux of the [Ne II] 12.8-μm line measured with the

SWS (see Section 2), we obtain a Ne^+/H^+ abundance ratio of 1.38×10^{-5}. Similarly, our optical measurement of the [Ne IV] $\lambda\lambda 4724, 4726$ lines (Table 2), which have a total intensity of 2.99×10^{-4} relative to Hβ, yields a Ne^{3+}/H^+ ratio of 2.28×10^{-5}. Thus if we adopt the average abundance of $Ne^{2+}/H^+ = 1.37 \times 10^{-4}$ derived from the [Ne III] optical forbidden lines and infrared fine-structure lines, the total elemental abundance of Ne/H derived from CELs is therefore 1.74×10^{-4} or 8.24 on a logarithmic scale where H = 12.0. This value is slightly higher than the solar value of 8.09 (Anders & Grevesse 1989; Grevesse & Noels 1993) but agrees very well with the average Ne abundance of 8.18 deduced from a CEL analysis of a large sample of Galactic PN (Kingsburgh & Barlow 1994).

ORL abundance ratios for Ne^+/H^+ and Ne^{3+}/H^+ are not available. If we assume that the fraction of neon in these two ionization stages is the same as given by the CELs, then the average Ne^{2+}/H^+ abundance ratio of 5.44×10^{-4} derived from the ORLs listed in Tables 4 and 5 implies an ORL Ne/H abundance ratio of 6.91×10^{-4}, or 8.84 in units where H = 12.0, i.e. a factor of 5.6 higher than the solar abundance.

REFERENCES

Anders E., Grevesse N., 1989, Geochim. Cosmochim. Acta, 53, 197
Balick B., Alexander J., Hajian A. R., Terzian Y., Perinotto M., Patriarchi P., 1998, AJ, 116, 360
Brocklehurst M., 1972, MNRAS, 157, 211
Cahn J. H., Kaler J. B., Stanghellini L., 1992, A&AS, 94, 399
Condon J. J., Kaplan D. L., 1998, ApJS, 117, 361
Grevesse N., Noels A., 1993, in Prantzos N., Vangioni-Flam E., Cassé M., eds, Origin and Evolution of the Elements. Cambridge Univ. Press, Cambridge, p. 15
Kingsburgh R. L., Barlow M. J., 1994, MNRAS, 271, 257
Kisielius R., Storey P. J., Davey A. R., Neale L. T., 1998, A&AS, 133, 257
Leech K., 2000, The *ISO* handbook, Volume VI: The Short Wavelength Spectrometer. SAI/2000-008/Dc
Liu X.-W., Barlow M. J., Danziger I. J., Storey P. J., 1999, in Walsh J. R., Rosa M. R., eds, Proc. ESO Workshop on Chemical Evolution from Zero to High Redshift. Springer-Verlag, Berlin, p. 39
Liu X.-W, Barlow M. J., Cohen M., Danziger I. J., Luo S.-G., Baluteau J. P., Cox P., Emery R. J., Lim T., Péquignot D., 2001a, MNRAS, 323, 343
Liu X.-W., Danziger I. J., 1993, MNRAS, 263, 256
Liu X.-W., Luo S.-G., Barlow M. J., Danziger I. J., Storey P. J., 2001b, MNRAS, in press
Liu X.-W., Storey P. J., Barlow M. J., Clegg R. E. S., 1995, MNRAS, 272, 369
Liu X.-W., Storey P. J., Barlow M. J., Danziger I. J., Cohen M., Bryce M., 2000, MNRAS, 312, 585
Peimbert M., 1967, ApJ, 150, 825
Peimbert M., 1971, Bol. Obs. Tonantzintla y Tacubaya, 6, 29
Rubin R. H., Colgan S. W. J., Haas M. R., Lord S., Simpson J. P., 1997, ApJ, 479, 332
Storey P. J., Hummer D. G., 1995, MNRAS, 272, 41

This paper has been typeset from a T$_{E}$X/L^{A}T$_{E}$X file prepared by the author.